J. Plasma Phys. (2024), *vol*. 90, 905900602
Published by Cambridge University Press

doi:10.1017/S0022377824001375

Temperature anisotropy instabilities driven by intermittent velocity shears in the solar wind

Simon Opie [1],†, Daniel Verscharen [1], Christopher H.K. Chen [2], Christopher J. Owen [1], Philip A. Isenberg [3], Luca Sorriso-Valvo [4,5], Luca Franci [6] and Lorenzo Matteini [7]

[1]Mullard Space Science Laboratory, University College London, Dorking RH5 6NT, UK

[2]Department of Physics and Astronomy, Queen Mary University of London, London E1 4NS, UK

[3]Space Science Center, University of New Hampshire, Durham, NH 03824, USA

[4]CNR, Istituto per la Scienza e la Tecnologia dei Plasmi, via Amendola 122/D, 70126 Bari, Italy

[5]Space and Plasma Physics, School of Electrical Engineering and Computer Science, KTH Royal Institute of Technology, Teknikringen 31, 11428 Stockholm, Sweden

[6]Department of Mathematics, Physics and Electrical Engineering, Northumbria University, Newcastle upon Tyne NE1 8ST, UK

[7]The Blackett Laboratory, Department of Physics, Imperial College London, London SW7 2AZ, UK

(Received 21 May 2024; revised 27 September 2024; accepted 1 October 2024)

Where and under what conditions the transfer of energy between electromagnetic fields and particles takes place in the solar wind remains an open question. We investigate the conditions that promote the growth of kinetic instabilities predicted by linear theory to infer how turbulence and temperature-anisotropy-driven instabilities are interrelated. Using a large dataset from Solar Orbiter, we introduce the radial rate of strain, a novel measure computed from single-spacecraft data, which we interpret as a proxy for the double-adiabatic strain rate. The solar wind exhibits high absolute values of the radial rate of strain at locations with large temperature anisotropy. We measure the kurtosis and skewness of the radial rate of strain from the statistical moments to show that it is non-Gaussian for unstable intervals and increasingly intermittent at smaller scales with a power-law scaling. We conclude that the velocity field fluctuations in the solar wind contribute to the presence of temperature anisotropy sufficient to create potentially unstable conditions.

Keywords: space plasma physics, plasma instabilities, plasma nonlinear phenomena

1. Introduction

The solar wind is a weakly collisional, magnetised plasma characterised by kinetic processes that influence its dynamic evolution in ways that are not fully understood. The expansion of the solar wind into interplanetary space in the presence of a

† Email address for correspondence: simon.opie.18@ucl.ac.uk

decreasing background magnetic field (Matteini *et al.* 2007, 2012) implies that the particle distributions should be highly anisotropic by the time the plasma reaches a distance of ∼1 au from the Sun (Verscharen *et al.* 2016). The double-adiabatic (CGL; Chew, Low & Goldberger 1956) expansion of the solar wind predicts a decline in $T_\perp/T_\parallel$ with distance from the Sun, where $T_\perp$ ($T_\parallel$) is the proton temperature perpendicular (parallel) to the magnetic field direction (Matteini *et al.* 2007; Cranmer *et al.* 2009). However, observations at 1 au show that the solar wind is, on average, almost isotropic with respect to the background magnetic field, albeit with significant variability in temperature anisotropy about the isotropic equilibrium (Marsch *et al.* 1982; Kasper, Lazarus & Gary 2002; Bale *et al.* 2009; Maruca, Kasper & Bale 2011; Isenberg, Maruca & Kasper 2013; Coburn, Chen & Squire 2022).

The presence of temperature anisotropy in the solar wind is also linked to turbulence. Solar-wind turbulence facilitates a nonlinear transfer of energy from larger to smaller scales via a Kolmogorov-like inertial range, leading to the dissipation of energy at kinetic scales (Kolmogorov 1941; Alexandrova *et al.* 2013; Bruno & Carbone 2013; Kiyani, Osman & Chapman 2015; Chen 2016; Marino & Sorriso-Valvo 2023). This nonlinear energy transfer occurs via a cascade which is inherently anisotropic in the distribution of its spectral power with respect to the wavevector of the fluctuations, with $k_\perp \gg k_\parallel$, where $k_\perp$ ($k_\parallel$) is the component of the wavevector perpendicular (parallel) to the magnetic field direction (Cho & Vishniac 2000; Schekochihin *et al.* 2009; Wicks *et al.* 2011; Horbury, Wicks & Chen 2012; Oughton *et al.* 2015; Chen *et al.* 2016; Schekochihin 2022). Some solar wind models predict that the turbulent cascade is responsible for the temperature-anisotropic heating of the plasma (Parashar *et al.* 2009; Chandran *et al.* 2010; Howes 2015). Considering the expectations based on CGL expansion and temperature-anisotropic heating models, the observation of, on average, approximately isotropic plasma conditions suggests that additional processes act to restore isotropy through the transfer of energy (Marsch *et al.* 1982). The stability of the solar wind depends on the simultaneous contributions of all species in the plasma to its free energy (Chen *et al.* 2016), but here we consider only the protons.

A class of kinetic instabilities is triggered when the proton temperature anisotropy exceeds certain thresholds for the production of plasma waves and non-propagating modes. These instabilities transfer energy from the particles to electromagnetic fields and this transfer restores the proton distribution towards a stable state closer to isotropy (Gary 1976, 1993; Hellinger *et al.* 2006). At large scales, compressive fluctuations can drive temperature anisotropy leading to wave-driven instabilities that eventually reduce anisotropy through pitch-angle scattering of protons (Verscharen *et al.* 2016), while at small scales, kinetic instabilities predicted by linear theory redistribute energy through wave–particle interaction (Gary 1993; Kasper *et al.* 2002; Hellinger *et al.* 2011, 2013; Howes 2015).

Proton-kinetic processes, such as temperature-anisotropy-driven instabilities, predominantly occur on scales near the small-scale end of the inertial range of the plasma turbulence (Gary 2015). In contrast to the framework of traditional linear theory, kinetic instabilities in the solar wind operate in inhomogeneous and non-constant conditions due to the ubiquitous solar-wind turbulence (Coleman 1968; Frisch, Sulem & Nelkin 1978; Tu & Marsch 1995; Chen 2016; Verscharen, Klein & Maruca 2019; Opie *et al.* 2022, 2023). In developing a more robust understanding of where and under what conditions energy transfer takes place, it is therefore important to fully capture the interplay between kinetic and turbulent features at the appropriate scales in the solar wind (Osman *et al.* 2012; Chen 2016; Sorriso-Valvo *et al.* 2018*a*; Opie *et al.* 2022, 2023; Arzamasskiy *et al.* 2023).

https://doi.org/10.1017/S0022377824001375 Published online by Cambridge University Press

The solar-wind turbulence is intermittent and consistent with the model of multifractality (Frisch & Kolmogorov 1995), meaning that the fluctuations at different scales are not equally space-filling and instead contain coherent structures such as current sheets and velocity shear layers (Sorriso-Valvo *et al.* 1999; Greco *et al.* 2008; Osman *et al.* 2013; Servidio *et al.* 2014; Matthaeus *et al.* 2015; Qudsi *et al.* 2020). These structures extend across scales in the inertial range and exhibit a statistical scaling relationship that indicates that they are self-affine (Carbone, Veltri & Bruno 1995; Carbone, Bruno & Veltri 1996; Sorriso-Valvo *et al.* 1999; Kiyani, Chapman & Hnat 2006; Hnat *et al.* 2007).

We hypothesise that the turbulent and intermittent velocity field in the solar wind is dynamically important for driving the temperature anisotropy of the plasma protons. Using a large observational dataset, we localise conditions in the solar wind at and beyond the thresholds for the proton-driven oblique firehose instability when $T_\perp/T_\parallel < 1$ (Hellinger & Trávníček 2008; Markovskii & Vasquez 2022) and mirror-mode instability when $T_\perp/T_\parallel > 1$ (Kunz, Schekochihin & Stone 2014; Hellinger *et al.* 2017), which place effective boundaries for temperature anisotropy in the solar wind (Hellinger *et al.* 2006; Bale *et al.* 2009; Gary 2015). Working directly from the dynamical equations, we develop and analyse a quantitative measure for the impact of velocity shears on the temperature anisotropy: the radial rate of strain. We measure the third and fourth statistical moments of the radial rate of strain, the velocity field and the magnetic field, from which we infer where, in terms of turbulent structures in the solar wind, these instabilities are located.

We set out details of our data analysis in § 2. In § 3, we develop and evaluate our novel measure of the radial rate of strain, a one-dimensional proxy for the three-dimensional double-adiabatic strain rate. In § 4, we calculate the skewness and kurtosis of the radial rate of strain, the magnetic field and the velocity field. We discuss the significance of our results in § 5 and conclude with recommendations for further work in § 6.

2. Data analysis

2.1. *Dataset*

Our dataset, which is a significant extension of that used by Opie *et al.* (2022), comprises ≈1.5M datapoints, as detailed in table 1. Our data are taken from the Solar Orbiter public archive.[1] We use data from two of the *in situ* instruments on board the spacecraft which make measurements of the solar wind; namely the magnetic-field vector from the Magnetometer (MAG) at 8 Hz cadence (Horbury *et al.* 2020) and the proton moments from the Proton–Alpha Sensor (PAS). For the periods discussed here, PAS takes a 1 s sample every 4 s. PAS is part of the Solar Wind Analyser (SWA) instrument suite (Owen *et al.* 2020). For this study, we work in the (R, T, N) coordinate system, where the axis R points radially outwards from the Sun, T is given by the cross-product between the Sun's rotation vector and R, and N completes the right-handed triad.

The relative error for the PAS data is ≈0.27 % for the velocity measurements (Louarn *et al.* 2021). For our dataset, this represents an average absolute error of $\approx 1.2\,\mathrm{km\,s^{-1}}$.

Since we employ two-point field increments in this analysis, we use continuous data intervals of 4–7 days duration, subject to data availability. We exclude PAS datapoints for which the solar wind bulk velocity $<325\,\mathrm{km\,s^{-1}}$ or when measurements are outside the recommended PAS quality factor ≤ 0.2. No attempt is made to eliminate any structures, such as shocks or interplanetary coronal mass ejections (ICMEs), from the dataset. Reference to the Helio4Cast catalogue[2] for ICMEs observed by Solar Orbiter gives three ICMEs in total within our combined dataset. These occurred on 06 May 2021, 10 May 2021

[1] http://soar.esac.esa.int/soar/

[2] https://helioforecast.space/static/sync/icmecat/HELIO4CAST_ICMECAT_v22.csv

https://doi.org/10.1017/S0022377824001375 Published online by Cambridge University Press

Interval	Heliocentric distance (R_S)	Number of datapoints
07–18 October 2020	205	185 923
22–28 April 2021	190	131 481
05–11 May 2021	180	131 849
10–13 June 2021	200	79 641
06–11 July 2021	190	117 427
20–24 July 2021	180	88 429
09–12 October 2021	150	81 362
19–26 October 2021	160	159 404
02–07 November 2021	175	132 750
09–14 November 2021	180	86 201
16–19 November 2021	190	85 833
28 December 2021–02 January 2022	215	128 048
04–08 January 2022	215	58 773

TABLE 1. Data selection from the Solar Orbiter Archive with approximate heliocentric distance (in solar radii, R_S) for each data interval.

and 03 November 2021 for an aggregated duration of 79.16 hours of our total observational time frame of 80 days (Möstl *et al.* 2017, 2020).

Solar Orbiter provides a continuous high-resolution dataset of the pristine solar wind for both magnetic and proton velocity field analysis (Louarn *et al.* 2021). This enables our two-point field increment method to be statistically robust on time scales that are equivalent to the scales needed to observe unstable intervals (Opie *et al.* 2022).

2.2. *Data processing*

We rotate the proton pressure tensor to align with the local associated magnetic field and create a time series for $\beta_\parallel \equiv 8\pi n_p k_B T_\parallel / B^2$, where n_p is the proton number density, k_B is the Boltzmann constant and B is the magnetic field strength averaged over the associated 1 s PAS measurement interval. From the proton pressure tensor, we then calculate the ratio $T_\perp / T_\parallel$ for each PAS measurement.

To identify intervals in our dataset for which linear theory predicts the growth of kinetic instabilities, we require thresholds for the growth of the specific anisotropy-driven kinetic instabilities of interest. We base our identification of unstable intervals on the parametric approximation for the instability thresholds in the form

$$\frac{T_\perp}{T_\parallel} = 1 + \frac{a}{(\beta_\parallel - c)^b}, \tag{2.1}$$

where a, b and c are constants with values given for each instability for a range of instability maximum growth rates by Verscharen *et al.* (2016). We use the constants given for a maximum growth rate of $\gamma_m = 10^{-2}\Omega_p$, where Ω_p is the proton gyrofrequency. We evaluate these instability thresholds for the oblique firehose (OF) and for the mirror-mode (M) instabilities. For reference, we also include the instability threshold for the Alfvén/ion-cyclotron (A/IC) instability in part of our analysis.

We analyse data distributed in $T_\perp/T_\parallel$–$\beta_\parallel$ parameter space that is bounded by these thresholds. We define the unstable intervals as comprising those data points that lie above the thresholds, while we characterise all data below the thresholds as stable. Consequently, the plasma is considered unstable against M and A/IC instabilities if $T_\perp/T_\parallel$ is greater than

https://doi.org/10.1017/S0022377824001375 Published online by Cambridge University Press

the value given by the right-hand side of (2.1), while it is considered unstable against the OF instability if $T_\perp/T_\parallel$ is less than the value given by the right-hand side of (2.1) with, in each case, the constants chosen for the respective instability.

3. Radial strain

In this section, we use a single-species (proton) fluid model of space plasma that derives anisotropy directly from the effect of fluid strain on the pressure tensor. We define the radial rate of strain Γ_R as a proxy for the strain rate in fully three-dimensional turbulence for this analysis, which we believe to be a novel technique. We then use this measure to test our hypothesis that intermittent velocity shear is dynamically important for the generation of the observed temperature anisotropy in the solar wind.

3.1. *Method: determination of the radial strain*

We examine the evolution of pressure anisotropy based on the first three moments of the proton distribution function under CGL analysis (Chew *et al.* 1956; Kulsrud 1984). We take the form of the equation for pressure anisotropy given by Squire *et al.* (2023) which assumes that the pressure tensor is invariant to rotation about the magnetic field direction:

$$\frac{\mathrm{d}}{\mathrm{d}t}(p_\perp - p_\parallel) = (p_\perp + 2p_\parallel)\hat{\boldsymbol{b}}\hat{\boldsymbol{b}} : \boldsymbol{\nabla v} - (2p_\perp - p_\parallel)\boldsymbol{\nabla}\cdot\boldsymbol{v} \\ -\boldsymbol{\nabla}\cdot[(q_\perp - q_\parallel)\hat{\boldsymbol{b}}] - 3q_\perp\boldsymbol{\nabla}\cdot\hat{\boldsymbol{b}} - \nu_c(p_\perp - p_\parallel), \tag{3.1}$$

where $p_\perp$ and $p_\parallel$ are the proton pressure tensor components perpendicular and parallel to the magnetic field, $\hat{\boldsymbol{b}} = \boldsymbol{B}/B$, $\boldsymbol{v}$ is the proton bulk velocity, $q_\perp$ and $q_\parallel$ are the proton heat fluxes perpendicular and parallel to the magnetic field direction, and ν_c is the proton collisional relaxation frequency for temperature anisotropy. The first two terms on the right-hand side of (3.1) describe how plasma bulk flows directly affect pressure anisotropy through shear and compression. We assume that $\nu_c = 0$ and $q_\perp = q_\parallel = 0$ following the arguments of Del Sarto & Pegoraro (2018).

These assumptions allow us to formulate a new proxy measure for the driving of pressure anisotropy by plasma motion based on plasma measurements sampled along the radial direction by a single spacecraft. We use Taylor's hypothesis (Taylor 1938) to transpose spatial partial derivatives to temporal partial derivatives and employ increments to replace $\boldsymbol{\nabla}\cdot\boldsymbol{v}$ and $\boldsymbol{\nabla v}$. After these transformations, we define the radial rate of strain as

$$\Gamma_R = \frac{1}{\tau}\left\{\left[(p_\perp + 2p_\parallel)\left(\hat{b}_R\hat{b}_R\Delta v_R + \hat{b}_T\hat{b}_R\Delta v_T + \hat{b}_N\hat{b}_R\Delta v_N\right)\right] - (2p_\perp - p_\parallel)\Delta v_R\right\}, \tag{3.2}$$

where τ is the time increment between measurement points (i.e. the measurement cadence) and $\Delta\phi$ denotes the scale-dependent increment $\Delta\phi = \phi(t) - \phi(t+\tau)$ of any time-dependent observable ϕ in the spacecraft reference frame.

Following the interpretation of the first and second terms in (3.1), we decompose (3.2) into proxies for the incompressible (Γ_{RI}) and compressible (Γ_{RC}) contributions to Γ_R as

$$\Gamma_{RI} \equiv \frac{1}{\tau}\left[(p_\perp + 2p_\parallel)\left(\hat{b}_R\hat{b}_R\Delta v_R + \hat{b}_T\hat{b}_R\Delta v_T + \hat{b}_N\hat{b}_R\Delta v_N\right)\right] \tag{3.3}$$

and

$$\Gamma_{RC} \equiv \frac{1}{\tau}\left[(p_\parallel - 2p_\perp)\Delta v_R\right]. \tag{3.4}$$

https://doi.org/10.1017/S0022377824001375 Published online by Cambridge University Press

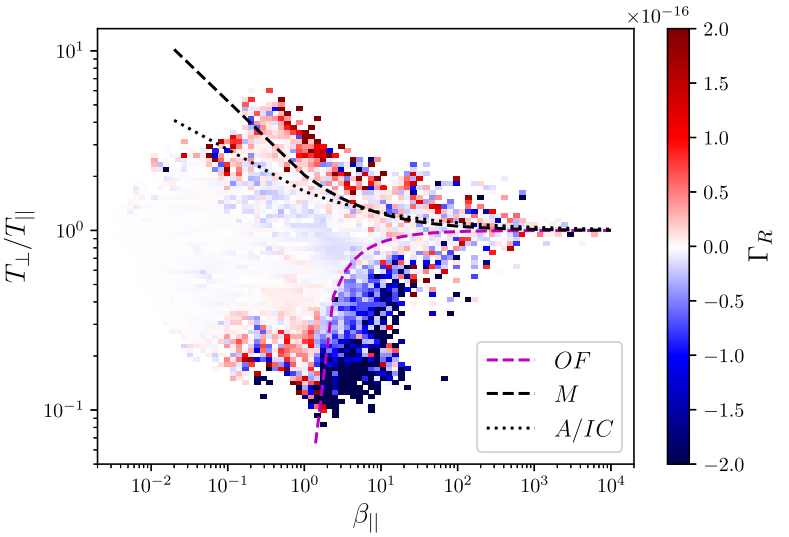

FIGURE 1. Distribution of Γ_R as bin averages in $T_\perp/T_\parallel$–$\beta_\parallel$ parameter space. We overplot the instability thresholds for the oblique firehose (OF), Alfvén/ion-cyclotron (A/IC) and mirror-mode (M) instabilities.

We set $\tau = 8$ s, which results in an average relative value of $\Delta v_j/|\boldsymbol{v}|$ for our intervals of 0.48 %. We check that all data with small Δv_j values make a negligible contribution to Γ_R and so the relevant datapoints are well above the PAS relative error. Any systematic errors due to bias offsets in any quantity ϕ are eliminated through the process of calculating the difference $\Delta\phi$. We exclude any data points for which an increment of $\tau = 8$ s cannot be calculated due to data gaps.

3.2. *Results: the radial strain of stable and unstable plasma intervals*

We calculate Γ_R from (3.2) for each datapoint in our dataset after the elimination of data gaps and plot the bin-averaged values in a two-dimensional histogram in $T_\perp/T_\parallel$–$\beta_\parallel$ parameter space in figure 1. We also calculate Γ_{RI} from (3.3) and Γ_{RC} from (3.4), and plot these separately in two-dimensional histograms in $T_\perp/T_\parallel$–$\beta_\parallel$ parameter space in figures 2 and 3, respectively.

According to figure 1, the unstable intervals show, on average, high absolute values, relative to the stable data, of Γ_R, with $\Gamma_R > 0$ in the parameter space associated with the M and A/IC instabilities and $\Gamma_R < 0$ in the parameter space associated with the OF instability. This relation is equally maintained for both Γ_{RI} and Γ_{RC}, as shown in figures 2 and 3, although the signal varies with $\beta_\parallel$ and $T_\perp/T_\parallel$. The contribution from Γ_{RC} is important at lower $\beta_\parallel$ and higher $T_\perp/T_\parallel$ for the mirror-mode unstable region of parameter space and at lower values of $T_\perp/T_\parallel$ for the oblique firehose unstable region. For the stable data, the average value of Γ_R is $\sim$0 except for the boundary regions of stable parameter space where either $T_\perp/T_\parallel < 0.3$ or $T_\perp/T_\parallel > 2$. This result is consistent for both Γ_{RI} and Γ_{RC}, although we see some variance in the sign of Γ_{RI} at the boundary to the mirror-mode unstable region.

We verify from the probability density functions (not shown here) of Γ_R for each of the stable (Γ_R^S), oblique firehose unstable (Γ_R^{OF}) and mirror-mode unstable (Γ_R^M) regions that the magnitude of the averaged Γ_R is consistently larger in the unstable measurement intervals and that the contrast with the stable region is not simply an

https://doi.org/10.1017/S0022377824001375 Published online by Cambridge University Press

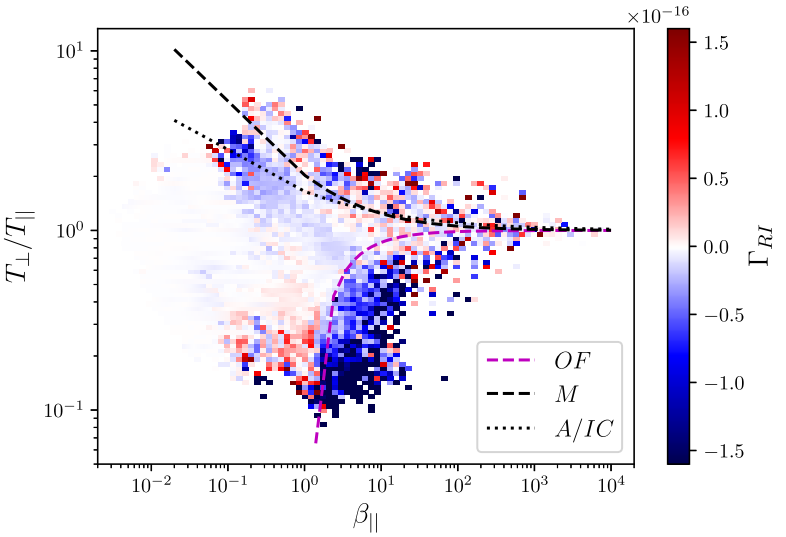

FIGURE 2. Distribution of Γ_{RI} as bin averages in $T_\perp/T_\parallel$–$\beta_\parallel$ parameter space. We overplot the instability thresholds for the oblique firehose (OF), Alfvén/ion-cyclotron (A/IC) and mirror-mode (M) instabilities.

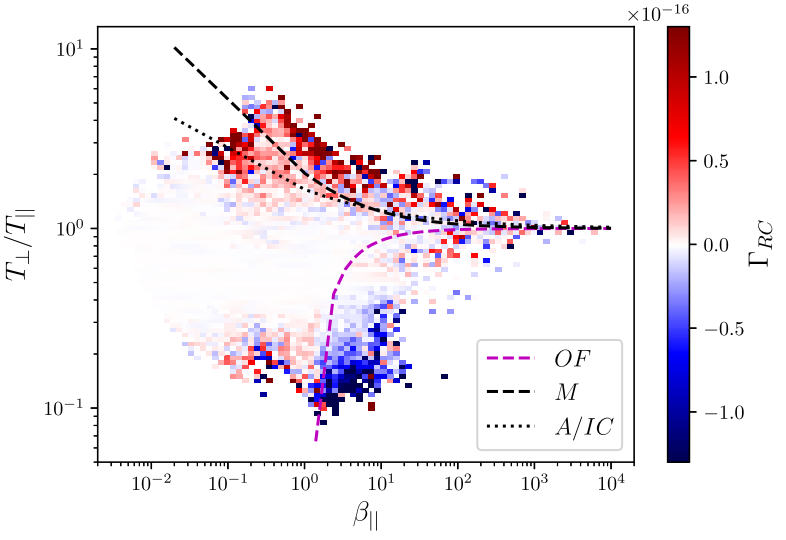

FIGURE 3. Distribution of Γ_{RC} as bin averages in $T_\perp/T_\parallel$–$\beta_\parallel$ parameter space. We overplot the instability thresholds for the oblique firehose (OF), Alfvén/ion-cyclotron (A/IC) and mirror-mode (M) instabilities.

averaging effect. We find the mean values as $\langle \Gamma_R^S \rangle = -3.76 \times 10^{-18}\,\mathrm{J\,cm^3\,s^{-1}}$, $\langle \Gamma_R^{OF} \rangle = -4.95 \times 10^{-17}\,\mathrm{J\,cm^3\,s^{-1}}$ and $\langle \Gamma_R^M \rangle = 3.51 \times 10^{-17}\,\mathrm{J\,cm^3\,s^{-1}}$, where $\langle \cdot \rangle$ represents the average over all measurement intervals in the respective category.

https://doi.org/10.1017/S0022377824001375 Published online by Cambridge University Press

	κ_i	κ_i^S	κ_i^{OF}	κ_i^M	λ_i	λ_i^S	λ_i^{OF}	λ_i^M
Γ_R	6.97×10^4	4.78×10^3	1.65×10^4	4.17×10^3	-134	-4.03	-117	$+61.7$
$\boldsymbol{v}$	4.78	4.84	2.69	2.43	$+1.05$	$+1.07$	$+0.31$	$+0.602$
$\boldsymbol{B}$	16.0	15.8	3.26	4.43	$+2.86$	$+2.86$	$+0.389$	$+0.816$

TABLE 2. Skewness λ_i and kurtosis κ_i for Γ_R, $\boldsymbol{v}$ and $\boldsymbol{B}$ across all data, stable intervals and unstable intervals.

4. Intermittency

In this section, we analyse statistical moments, specifically the third (skewness) and fourth (kurtosis) moments, to measure the intermittency of Γ_R. We compare this result with the skewness and kurtosis of the background magnetic and velocity fields.

Intermittency of magnetic and electric fields and plasma parameters (velocity, density, temperature) in the inertial range has been extensively studied (Tu & Marsch 1995; Marsch & Tu 1997; Sorriso-Valvo *et al.* 1999; Bruno *et al.* 2001). We examine the statistical measures separately for stable and unstable intervals to understand the dynamics of the driving of anisotropy by the turbulent fluctuations. In particular, we investigate how the intermittency (in the sense of 'burstiness') of the pressure strain varies across the relevant scales.

4.1. *Method: measuring the skewness and kurtosis across scales*

We use the statistical moments of the quantities μ_i to calculate their skewness λ_i and their kurtosis κ_i, where μ_i is the moment about the mean. The skewness and kurtosis are defined as

$$\lambda_i = \frac{\langle \mu_i^3 \rangle}{\langle \mu_i^2 \rangle^{3/2}} \tag{4.1}$$

and

$$\kappa_i = \frac{\langle \mu_i^4 \rangle}{\langle \mu_i^2 \rangle^2}. \tag{4.2}$$

Using (4.1) and (4.2), we calculate λ_i and κ_i for Γ_R, $\boldsymbol{B}$ and $\boldsymbol{v}$. We calculate λ_i and κ_i for the whole dataset and for each of the stable, oblique firehose unstable and mirror-mode unstable datasets.

We also calculate λ_{Γ_R} and κ_{Γ_R} across a range of temporal scales. We do this by creating scale-dependent datasets for Γ_R using (3.2) with $\tau \in \{8\,\mathrm{s}, 16\,\mathrm{s}, 32\,\mathrm{s}, 64\,\mathrm{s}, 128\,\mathrm{s}, 256\,\mathrm{s}, 512\,\mathrm{s}, 1024\,\mathrm{s}, 2048\,\mathrm{s}\}$. This results in scale-dependent values of λ_{Γ_R} and κ_{Γ_R} from the small-scale end of the inertial range up to the correlation-length scale.

4.2. *Results: the intermittency of Γ_R*

We show the values obtained for λ_i and κ_i in table 2. The values of λ_i indicate a symmetric distribution in nearly all cases except for $\lambda_{\Gamma_R}^{OF}$ which is strongly negative and $\lambda_{\Gamma_R}^{M}$ which is strongly positive, while the overall λ_{Γ_R} is also strongly negative.

We see that $\kappa_{\Gamma_R} \gg \kappa_{\boldsymbol{v}}$ and $\kappa_{\Gamma_R} \gg \kappa_{\boldsymbol{B}}$; in both cases, by 2–3 orders of magnitude. This is expected since Γ_R is built by multiplying intermittent quantities, and its normalised moments will therefore correspond to higher-order moments when compared with $\boldsymbol{v}$ and $\boldsymbol{B}$. For the conditioned subsets of Γ_R, $\kappa_{\Gamma_R}^{OF} > \kappa_{\Gamma_R}^{S} \approx \kappa_{\Gamma_R}^{M}$.

https://doi.org/10.1017/S0022377824001375 Published online by Cambridge University Press

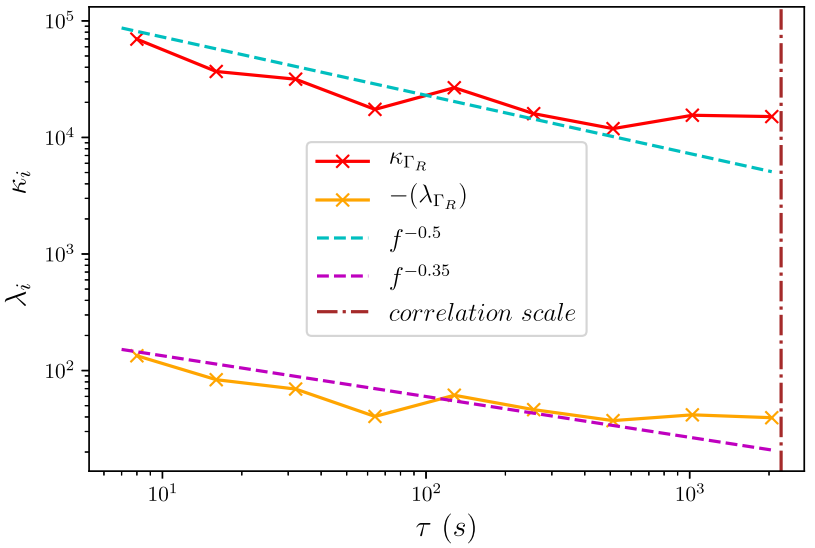

FIGURE 4. λ_{Γ_R} and κ_{Γ_R} over a range of temporal scales τ from 8 s to 2048 s. The cyan and magenta dashed lines represent a power-law scaling of -0.5 and -0.35, respectively. The brown vertical dash-dotted line represents the correlation scale.

We calculate λ_i and κ_i for Γ_{RI} and Γ_{RC}. Here, $\lambda_{\Gamma_{RI}} \approx -104$ is negative while $\lambda_{\Gamma_{RC}} \approx +46$ is positive. Additionally, $\kappa_{\Gamma_{RI}} \approx 5.1 \times 10^4$ and $\kappa_{\Gamma_{RC}} \approx 3.05 \times 10^4$ are consistent with κ_{Γ_R}.

Figure 4 shows the scale-dependent values of λ_{Γ_R} and κ_{Γ_R} as functions of τ. Both λ_{Γ_R} and κ_{Γ_R} show a power-law scaling which is overlaid as indicated. The values for λ_{Γ_R} show that the skewness of Γ_R increases with decreasing scale from a local minimum at $\tau \approx 512$ s. The sign of all values of λ_{Γ_R} is negative and has been reversed for visualisation on the logarithmic axis.

The values of κ_{Γ_R} indicate that the burstiness of the Γ_R field increases with decreasing scale, which is the signature of scale-dependent statistics typical of intermittency. Over all τ in this figure, the Γ_R field is evidently intermittent and hence 'bursty' due to a heavy-tailed distribution of Γ_R. The value of κ_{Γ_R} reaches a local minimum at $\tau \approx 512$ s.

5. Discussion

Under the assumptions underlying (3.1) in § 3, shear and compression create pressure anisotropy (Squire *et al.* 2023), and we interpret our findings as being consistent with that prediction. Relative to the stable data, the absolute values of the bin-averaged Γ_R for the unstable data are significantly elevated, on average by a factor of ten. Our interpretation for this observation is that the presence of data in unstable intervals requires the pressure strain from turbulence-driven shears and compressions to compete with the instabilities that act to restore the plasma towards isotropy. In effect, data can only reside in unstable conditions if the time scale associated with the pressure-strain driving of temperature anisotropy is sufficiently small compared with the relaxation time of the relevant instabilities.

Previous work demonstrates that temperature anisotropy and vorticity are well correlated in hybrid simulations of plasma turbulence (Franci *et al.* 2016). Hybrid-kinetic simulations also show that oblique firehose and mirror-mode instabilities can be driven by a changing magnetic field in a shear flow (Kunz *et al.* 2014). Our results suggest that the turbulent shears in the velocity field create and modulate temperature anisotropy

https://doi.org/10.1017/S0022377824001375 Published online by Cambridge University Press

through a purely dynamical process such as that proposed by Del Sarto & Pegoraro (2018) and observed in near-Earth space (Servidio *et al.* 2014; Sorriso-Valvo *et al.* 2019). In this scenario, the non-compressive turbulent fluctuations result in spatially intermittent velocity shears that modulate the frozen-in magnetic field and drive $T_\perp/T_\parallel \neq 1$ with a corresponding change in magnetic field strength (Del Sarto, Pegoraro & Califano 2016; Del Sarto & Pegoraro 2018; Squire *et al.* 2023).

We also see a role for compressive fluctuations in this scenario as per figure 3, where the distribution of Γ_{RC} is similar to the distribution of Γ_R. Figure 3 also shows that the contribution from compressive fluctuations to Γ_R in unstable intervals has the highest absolute average values where $T_\perp/T_\parallel$ approaches its maximum (M) or minimum (OF) bounds. In particular, we infer from comparison with figure 2 that compressive fluctuations are important in driving temperature anisotropy that creates conditions unstable to the mirror-mode instability. This is consistent with previous findings concerning the distribution of magnetic field fluctuations in unstable intervals (Opie *et al.* 2023). We expect the contribution from Γ_{RC} to be less significant overall since compressive fluctuations only account for a minor fraction of the solar wind turbulent energy (Tu & Marsch 1995; Bruno & Carbone 2013; Verscharen *et al.* 2019; Marino & Sorriso-Valvo 2023).

The role of Γ_R in driving mirror-mode unstable conditions is further supported by the skewness of Γ_R and its conditioned subsets where, as set out in § 4, both $\lambda_{\Gamma_{RC}}$ and $\lambda^M_{\Gamma_R}$ are positive while λ_i is negative for the other subsets or close to zero for $\lambda^S_{\Gamma_R}$.

In the solar wind, the instabilities, once triggered, act on time scales that rapidly reduce the temperature anisotropy (Bandyopadhyay *et al.* 2022; Opie *et al.* 2022, 2023). The persistence of unstable intervals is, however, observable over extended spatial and temporal scales (Opie *et al.* 2022). Although we cannot fully exclude the possibility that Γ_R reflects the fluctuations created by the instabilities themselves rather than the anisotropy-driving background turbulence, this persistence time scale argument suggests that the temperature anisotropies are indeed driven by the plasma motions. In addition to the consideration of the magnitude of Γ_R, an analysis of the normalised cross-helicity and the Alfvén ratio shows that there are structural differences in the turbulence in the unstable regions (see Appendix A). This analysis suggests that there is an imbalance relative to the stable data whereby, on average, the energy in the velocity field is greater than that in the magnetic field for the unstable intervals. A further discussion of these structural differences would be worthwhile in a future study.

We note that our use of the radial rate of strain is distinct from the pressure strain interaction – the so-called Pi-D formalism – analysis that examines the contribution of turbulent fluctuations to the heating of ions (Yang *et al.* 2017; Bandyopadhyay *et al.* 2020; Yang *et al.* 2023). Nonetheless, our formulation goes some way to explaining the relationship between velocity shears and temperature anisotropy noted as an open question by Yang *et al.* (2017).

Similarly, our measure differs from the partial variation of increments (PVI), which is used to locate magnetic (or velocity) field structures in solar-wind turbulence (Greco *et al.* 2008, 2017). The radial rate of strain Γ_R is a dynamical measure that does not involve normalisation by a long-term average and is applied directly to fluctuations in the velocity field. We use Γ_R to identify the creation of temperature anisotropy. We calculate the Pearson correlation coefficients between PVI and Γ_R for our complete dataset and separately for each of the three conditioned subsets defined by stable, oblique firehose unstable and mirror-mode unstable intervals. We find negligible to no correlation with coefficients that range from $\approx$0.09 for the stable data to $\approx$0.003 for the whole dataset.

https://doi.org/10.1017/S0022377824001375 Published online by Cambridge University Press

Observations and simulations suggest an important role for turbulent structures in the evolution of plasma conditions in the solar wind (Osman *et al.* 2012; Servidio *et al.* 2014; Franci *et al.* 2015; Greco *et al.* 2017; Sorriso-Valvo *et al.* 2017; Hellinger *et al.* 2019; Qudsi *et al.* 2020). In § 4, we use statistical analysis to link the role of Γ_R in driving unstable conditions with the skewness and kurtosis of Γ_R, $\boldsymbol{B}$ and $\boldsymbol{v}$. We apply this analysis to the conditioned subsets denoted as stable, oblique firehose unstable and mirror-mode unstable. The large kurtosis of Γ_R and its subsets show that Γ_R is highly intermittent and exhibits burstiness to a greater degree than either $\boldsymbol{B}$ or $\boldsymbol{v}$. We see that $\kappa^{OF}_{\Gamma_R}$ is considerably greater than either $\kappa^{M}_{\Gamma_R}$ or $\kappa^{S}_{\Gamma_R}$, which is not the case for the subsets of $\boldsymbol{B}$ or $\boldsymbol{v}$.

Coupled with the values for the skewness, we find three distinct subsets of Γ_R with positively and negatively skewed subsets being associated with the oblique firehose and mirror-mode instabilities, respectively, whilst for the stable data, the skewness is nearly zero. The fact that the overall magnitudes of the skweness and kurtosis of Γ_R are greater than those for the individual subsets implies that additional intermittency comes precisely from the alternation of these three distinct regions of stable data, oblique firehose unstable data and mirror-mode unstable data.

The power-law scalings of λ_{Γ_R} and κ_{Γ_R}, shown in figure 4, follow an exponent that is compatible with standard intermittency in the solar-wind magnetic field (Sorriso-Valvo *et al.* 1999). This correspondence is not unexpected since Γ_R is built using various intermittent quantities. However, it implies that the greater magnitudes of λ_{Γ_R} and κ_{Γ_R} relative to those of $\boldsymbol{B}$ and $\boldsymbol{v}$ are not scale-dependent. We should therefore expect to see the regions of stable, oblique firehose unstable and mirror-mode unstable data characterised by distinct subsets of Γ_R across scales in the inertial range of solar-wind turbulence.

While it has long been known that the turbulence in the solar wind is intermittent and multifractal (Paladin & Vulpiani 1987; Burlaga 1991; Frisch & Kolmogorov 1995; Tu & Marsch 1995), the analysis of our statistically robust, large dataset quantifies these characteristics in a novel way, allowing us to treat separately stable and unstable intervals in the data. Calculation from observations of all the quantities in this study requires the use of incremental gradients, and we benefit from Solar Orbiter's *in situ* instrument suite that provides continuous high-resolution datasets over significant time scales to enable this. The scientific impacts of the efficiency and high resolution of these instruments are by now well documented (Rouillard *et al.* 2020; D'Amicis *et al.* 2021; Louarn *et al.* 2021; Opie *et al.* 2022). Nevertheless, our measures are restricted by the use of single-spacecraft data, which confines all analyses in this work to the radial sampling direction. In our view, the most promising route to extend this work lies in the use of high-quality three-dimensional data from a multi-spacecraft mission. This extension would allow the estimation of all relevant three-dimensional gradients rather than sampling along the radial direction via Taylor's hypothesis only. It would also be useful to extend the range of radial distances from the Sun over which these analyses are made using the perihelia data from Solar Orbiter and Parker Solar Probe.

Previous work shows how unstable intervals are statistically spatially and temporally distributed (Opie *et al.* 2022), and that unstable intervals are ergodicity-breaking and therefore statistically disjoint with respect to the stable regime (Opie *et al.* 2023). Our current findings support and extend these previous results and describe more fully the impact of turbulence on kinetic instabilities in the solar wind, and in particular quantify the role of Γ_R in driving unstable conditions.

https://doi.org/10.1017/S0022377824001375 Published online by Cambridge University Press

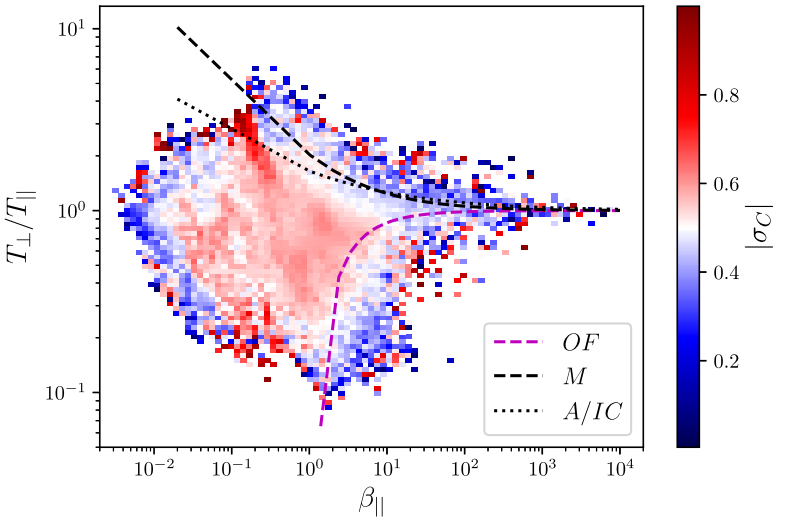

FIGURE 5. Distribution of $|\sigma_c|$ as bin averages in $T_\perp/T_\parallel$–$\beta_\parallel$ parameter space. We overplot the instability thresholds for oblique firehose (OF), Alfvén/ion-cyclotron (A/IC) and mirror-mode (M) instabilities.

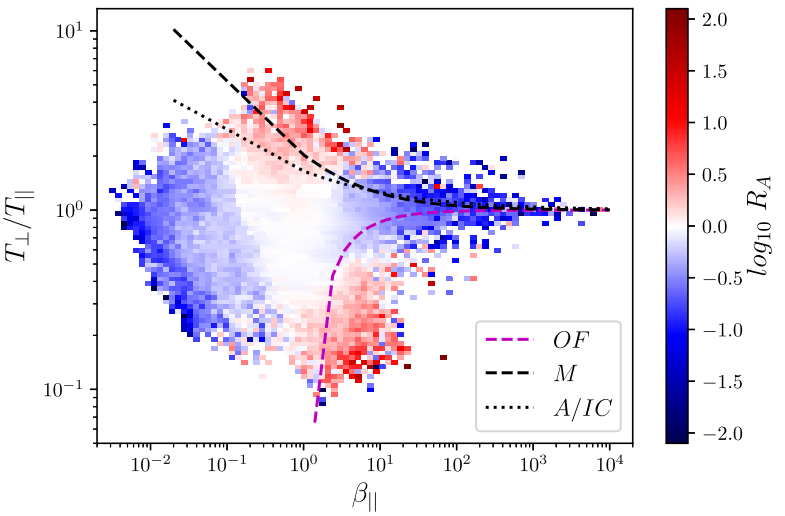

FIGURE 6. Distribution of R_A plotted as bin averages in $T_\perp/T_\parallel$–$\beta_\parallel$ parameter space with instability thresholds shown for oblique firehose (OF), Alfvén/ion-cyclotron (A/IC) and mirror-mode (M) instabilities.

6. Conclusions

In this work, we show that solar-wind intervals with parameters above the thresholds for temperature-anisotropy-driven instabilities are on average characterised by high absolute values of Γ_R which is a measure of the extent to which bulk motions in the plasma drive temperature anisotropy. We attribute this observational result to the proposition that strong velocity shears drive temperature anisotropies in the turbulent solar wind through the

https://doi.org/10.1017/S0022377824001375 Published online by Cambridge University Press

shearing of the frozen-in magnetic field with a double-adiabatic impact on the particle distributions.

The radial rate of strain Γ_R is highly intermittent with a distribution that exhibits greater levels of kurtosis relative to those of $\boldsymbol{B}$ and $\boldsymbol{v}$, which is not unexpected given the contribution of increments of both $\boldsymbol{B}$ and $\boldsymbol{v}$ in (3.2). Nonetheless, we attribute this observational result to the burstiness of velocity shears in the solar wind with a significant occurrence rate of extreme values leading to a heavy-tailed distribution of Γ_R. The conditioned subsets of Γ_R that relate to stable, oblique firehose unstable and mirror-mode unstable intervals comprise distributions that are characteristically asymmetric (or symmetric in the case of stable data). The alternation of these distinct subsets contributes to the intermittency of Γ_R. We attribute this observational result to the inhomogeneity that distinguishes each of the three regions of $T_\perp/T_\parallel$–$\beta_\parallel$ parameter space represented by the subsets and that are both statistically and physically disjoint. Our observational measures – skewness and kurtosis – exhibit power-law scalings with an exponent that is consistent with the known intermittency in solar-wind turbulence.

Our study opens several areas of extended interest that deserve further exploration. For turbulence studies, our results emphasise the importance of the velocity field for the temperature anisotropy (and potentially other kinetic properties) of the plasma. We suggest that an analysis of the local energy transfer (LET) measure derived from the Politano–Pouquet scaling law (Politano & Pouquet 1998; Sorriso-Valvo *et al.* 2018*b*), revised to account for pressure-anisotropic magnetohydrodynamic turbulence (Simon & Sahraoui 2022), would be a useful extension of the current study. In addition, the role of Γ_R in solar-wind turbulence could be further investigated in the simulation domain, ideally building on the existing work that shows how fluctuations in the velocity field are related to anisotropy (Franci *et al.* 2015, 2016, 2018; Hellinger *et al.* 2019).

Our work highlights new science opportunities for multi-spacecraft missions such as HelioSwarm (Klein *et al.* 2023) and Plasma Observatory (Retinò *et al.* 2022), which will provide a means of measuring fully three-dimensional rates of strain and intermittency. These data will enable a more precise unpicking of the contributions of non-compressive and compressive fluctuations as well as intermittency to the creation and modulation of temperature anisotropy. A mission like HelioSwarm or Plasma Observatory with their complements of fields and plasma instrumentation has thus the potential to create breakthroughs in our understanding of the interplay between turbulence and kinetic instabilities in space plasmas. In particular, our results suggest that accurate and high-resolution measurements of the velocity field will be of fundamental importance to this task.

Our investigation of Solar Orbiter observations reveals a consistent picture of where and under what conditions kinetic instabilities act at the relevant scales in the turbulent solar wind. Unstable intervals are located in regions of strong velocity shear embedded in rapidly changing structures in the intermittent turbulence of the velocity field. The velocity shear and its associated impact on the frozen-in magnetic field drives and modulates the temperature anisotropy necessary to create the unstable conditions. The plasma can only remain above the instability thresholds for as long as the shears are sufficient to overcome the relaxation through the instabilities. This process takes place predominantly at the shear layers of highly intermittent structures whose distribution is strongly non-Gaussian. Accordingly, the presence of instabilities is not evenly distributed either spatially or temporally in the solar wind plasma.

Acknowledgements

Editor T. Passot thanks the referees for their advice in evaluating this article.

https://doi.org/10.1017/S0022377824001375 Published online by Cambridge University Press

Funding

S.O. is supported by NERC grant NE/S007229/1. D.V. and C.J.O. are supported by STFC Consolidated Grant ST/W001004/1. C.H.K.C. is supported by UKRI Future Leaders Fellowship MR/W007657/1 and STFC Consolidated Grants ST/T00018X/1 and ST/X000974/1. P.A.I. is supported by NSF grant AGS2005982. L.F. is supported by the Royal Society University Research Fellowship No. URF/R1/231710 and by UKRI/STFC grant ST/W001071/1. This research was discussed at the International Space Science Institute (ISSI) in Bern, through ISSI International Team project #563 (Ion Kinetic Instabilities in the Solar Wind in Light of Parker Solar Probe and Solar Orbiter Observations) led by L. Ofman and L. Jian. This work was supported by the Royal Society (UK) and the Consiglio Nazionale delle Ricerche (Italy) through the International Exchanges Cost Share scheme/Joint Bilateral Agreement project "Multi-scale electrostatic energisation of plasmas: comparison of collective processes in laboratory and space" (award numbers IEC\\R2\\222050 and SAC.AD002.043.021). Solar Orbiter is a space mission of international collaboration between ESA and NASA, operated by ESA. Solar Orbiter Solar Wind Analyser (SWA) data are derived from scientific sensors which have been designed, created and are operated under funding provided in numerous contracts from the UK Space Agency (UKSA), STFC, the Agenzia Spaziale Italiana (ASI), the Centre National d'Études Spatiales (CNES), the Centre National de la Recherche Scientifique (CNRS), the Czech contribution to the ESA PRODEX programme and NASA. Solar Orbiter SWA work at UCL/MSSL is currently funded under STFC grants ST/T001356/1 and ST/S000240/1. The Solar Orbiter magnetometer was funded by UKSA grant ST/T001062/1.

Declaration of interests

The authors report no conflict of interest.

Appendix A. Alfvénicity in the solar wind

For this analysis of the Alfvénicity, we consider the fluctuations on the scale of 2 min, which is at the small-scale end of the inertial range and captures the relevant scales for the persistence of unstable intervals (Opie *et al.* 2022). We define

$$\delta \boldsymbol{b} = \boldsymbol{B} - \|\boldsymbol{B}\| \tag{A1}$$

and

$$\delta \boldsymbol{v} = \boldsymbol{v} - \|\boldsymbol{v}\|, \tag{A2}$$

where $\|\cdot\|$ denotes the time average taken over a 2-minute interval centred on the time of the measurement of $\delta \boldsymbol{b}$ and $\delta \boldsymbol{v}$.

We define the normalised cross-helicity as

$$\sigma_c = \frac{2\,(\delta \boldsymbol{v} \cdot \delta \boldsymbol{b})}{\left(|\delta \boldsymbol{v}|^2 + |\delta \boldsymbol{b}|^2\right)} \tag{A3}$$

and the Alfvén ratio as

$$R_A = \frac{|\delta \boldsymbol{v}|^2}{|\delta \boldsymbol{b}|^2}. \tag{A4}$$

With these definitions, we create point-wise datasets for σ_c and R_A that allow us to investigate the correlations of the magnetic field and velocity field fluctuations at the scale of 2 min.

https://doi.org/10.1017/S0022377824001375 Published online by Cambridge University Press

We show $|\sigma_c|$ and R_A as bin-averaged distributions in $T_\perp/T_\parallel$–$\beta_\parallel$ parameter space for our whole dataset in figures 5 and 6.

On average, normalised cross-helicity in the solar wind is higher near the core of the stable dataset in this parameter space, and lower in the unstable intervals and at the low-$\beta_\parallel$ boundary of the stable data. The distribution of the bin-averaged Alfvén ratio shows that $|\delta \boldsymbol{v}|^2 \gg |\delta \boldsymbol{b}|^2$ in the unstable regions of parameter space when $T_\perp/T_\parallel \leq 0.6$ or $T_\perp/T_\parallel \geq 1.6$.

We see that σ_c is significantly lower on average in the unstable intervals relative to the stable data, suggesting an imbalance between the velocity and magnetic field fluctuations in the unstable regions of the $T_\perp/T_\parallel$–$\beta_\parallel$ parameter space. This is consistent with the hypothesis of a restriction on the amplitude of Alfvénic fluctuations in the limit of the oblique firehose instability (Squire, Quataert & Schekochihin 2016; Squire, Schekochihin & Quataert 2017) and suggests a similar mechanism may apply in the limit of the mirror-mode instability. The distribution of bin-averaged R_A demonstrates that in the unstable intervals, greater temperature anisotropy is associated with the dominance of energy in the velocity field over energy in the magnetic field so that $R_A \gg 1$.

REFERENCES

Alexandrova, O., Chen, C.H.K., Sorriso-Valvo, L., Horbury, T.S. & Bale, S.D. 2013 Solar wind turbulence and the role of ion instabilities. *Space Sci. Rev*. **178** (2–4), 101–139.

Arzamasskiy, L., Kunz, M.W., Squire, J., Quataert, E. & Schekochihin, A.A. 2023 Kinetic turbulence in collisionless high-beta plasmas. *Phys. Rev.* X **13** (2), 021014.

Bale, S.D., Kasper, J.C., Howes, G.G., Quataert, E., Salem, C. & Sundkvist, D. 2009 Magnetic fluctuation power near proton temperature anisotropy instability thresholds in the solar wind. *Phys. Rev. Lett*. **103** (21), 211101.

Bandyopadhyay, R., Matthaeus, W.H., Parashar, T.N., Yang, Y., Chasapis, A., Giles, B.L., Gershman, D.J., Pollock, C.J., Russell, C.T., Strangeway, R.J., *et al.* 2020 Statistics of kinetic dissipation in the Earth's magnetosheath: MMS observations. *Phys. Rev. Lett*. **124** (25), 255101.

Bandyopadhyay, R., Qudsi, R.A., Gary, S.P., Matthaeus, W.H., Parashar, T.N., Maruca, B.A., Roytershteyn, V., Chasapis, A., Giles, B.L., Gershman, D.J., *et al.* 2022 Interplay of turbulence and proton-microinstability growth in space plasmas. *Phys. Plasmas* **29** (10), 102107.

Bruno, R. & Carbone, V. 2013 The solar wind as a turbulence laboratory. *Liv. Rev. Sol. Phys*. **10**.

Bruno, R., Carbone, V., Veltri, P., Pietropaolo, E. & Bavassano, B. 2001 Identifying intermittency events in the solar wind. *Planet. Space Sci*. **49** (12), 1201–1210.

Burlaga, L.F. 1991 Intermittent turbulence in the solar wind. *J. Geophys. Res*. **96** (A4), 5847–5851.

Carbone, V., Bruno, R. & Veltri, P. 1996 Evidences for extended self-similarity in hydromagnetic turbulence. *Geophys. Res. Lett*. **23** (2), 121–124.

Carbone, V., Veltri, P. & Bruno, R. 1995 Experimental evidence for differences in the extended self-similarity scaling laws between fluid and magnetohydrodynamic turbulent flows. *Phys. Rev. Lett*. **75** (17), 3110–3113.

Chandran, B.D.G., Li, B., Rogers, B.N., Quataert, E. & Germaschewski, K. 2010 Perpendicular ion heating by low-frequency Alfvén-wave turbulence in the solar wind. *Astrophys. J*. **720** (1), 503–515.

Chen, C.H.K. 2016 Recent progress in astrophysical plasma turbulence from solar wind observations. *J. Plasma Phys*. **82** (6).

Chen, C.H.K., Matteini, L., Schekochihin, A.A., Stevens, M.L., Salem, C.S., Maruca, B.A., Kunz, M.W. & Bale, S.D. 2016 Multi-species measurements of the firehose and mirror instability thresholds in the solar wind. *Astrophys. J*. **825** (2), L26.

https://doi.org/10.1017/S0022377824001375 Published online by Cambridge University Press

Chew, G.F., Low, F.E. & Goldberger, M.L. 1956 The Boltzmann equation and the one-fluid hydromagnetic equations in the absence of particle collisions. *Proc. R. Soc. Lond.* A **236** (1204), 112–118.

Cho, J. & Vishniac, E.T. 2000 The anisotropy of magnetohydrodynamic Alfvénic turbulence. *Astrophys. J.* **539** (1), 273.

Coburn, J.T., Chen, C.H.K. & Squire, J. 2022 A measurement of the effective mean free path of solar wind protons. *J. Plasma Phys*. **88** (5), 175880502.

Coleman, P.J. Jr. 1968 Turbulence, viscosity, and dissipation in the solar-wind plasma. *Astrophys. J.* **153**, 371.

Cranmer, S.R., Matthaeus, W.H., Breech, B.A. & Kasper, J.C. 2009 Empirical constraints on proton and electron heating in the fast solar wind. *Astrophys. J.* **702** (2), 1604.

D'Amicis, R., Bruno, R., Panasenco, O., Telloni, D., Perrone, D., Marcucci, M.F., Woodham, L., Velli, M., De Marco, R., Jagarlamudi, V., *et al.* 2021 First solar orbiter observation of the Alfvénic slow wind and identification of its solar source. *Astron. Astrophys*. **656**, A21.

Del Sarto, D. & Pegoraro, F. 2018 Shear-induced pressure anisotropization and correlation with fluid vorticity in a low collisionality plasma. *Mon. Not. R. Astron. Soc*. **475** (1), 181–192.

Del Sarto, D., Pegoraro, F. & Califano, F. 2016 Pressure anisotropy and small spatial scales induced by velocity shear. *Phys. Rev.* E **93** (5), 053203.

Franci, L., Hellinger, P., Matteini, L., Verdini, A. & Landi, S. 2016 Two-dimensional hybrid simulations of kinetic plasma turbulence: current and vorticity vs proton temperature. *AIP Conf. Proc*. **1720** (1), 040003.

Franci, L., Landi, S., Matteini, L., Verdini, A. & Hellinger, P. 2015 High-resolution hybrid simulations of kinetic plasma turbulence at proton scales. *Astrophys. J.* **812** (1), 21.

Franci, L., Landi, S., Verdini, A., Matteini, L. & Hellinger, P. 2018 Solar wind turbulent cascade from MHD to sub-ion scales: large-size 3D hybrid particle-in-cell simulations. *Astrophys. J.* **853** (1), 26.

Frisch, U. & Kolmogorov, A.N. 1995 *Turbulence: the legacy of A.N. Kolmogorov*. Cambridge University Press.

Frisch, U., Sulem, P.-L. & Nelkin, M. 1978 A simple dynamical model of intermittent fully developed turbulence. *J. Fluid Mech*. **87** (4), 719–736.

Gary, S.P. 1976 Proton temperature anisotropy instabilities in the solar wind. *J. Geophys. Res*. **81** (7), 1241–1246.

Gary, S.P. 1993 *Theory of Space Plasma Microinstabilities*. Cambridge Atmospheric and Space Science Series, vol. 7. Cambridge University Press.

Gary, S.P. 2015 Short-wavelength plasma turbulence and temperature anisotropy instabilities: recent computational progress. *Phil. Trans. R. Soc.* A **373** (2041), 20140149.

Greco, A., Chuychai, P., Matthaeus, W.H., Servidio, S. & Dmitruk, P. 2008 Intermittent MHD structures and classical discontinuities. *Geophys. Res. Lett*. **35** (19).

Greco, A., Matthaeus, W.H., Perri, S., Osman, K.T., Servidio, S., Wan, M. & Dmitruk, P. 2017 Partial variance of increments method in solar wind observations and plasma simulations. *Space Sci. Rev*. **214** (1), 1.

Hellinger, P., Landi, S., Matteini, L., Verdini, A. & Franci, L. 2017 Mirror instability in the turbulent solar wind. *Astrophys. J.* **838** (2), 158.

Hellinger, P., Matteini, L., Landi, S., Franci, L., Verdini, A. & Papini, E. 2019 Turbulence versus fire-hose instabilities: 3D hybrid expanding box simulations. *Astrophys. J.* **883** (2), 178.

Hellinger, P., Matteini, L., Štverák, Š., Trávníček, P.M. & Marsch, E. 2011 Heating and cooling of protons in the fast solar wind between 0.3 and 1 AU: Helios revisited. *J. Geophys. Res*. **116** (A9).

Hellinger, P. & Trávníček, P.M. 2008 Oblique proton fire hose instability in the expanding solar wind: hybrid simulations. *J. Geophys. Res*. **113** (A10).

Hellinger, P., Trávníček, P., Kasper, J.C. & Lazarus, A.J. 2006 Solar wind proton temperature anisotropy: linear theory and WIND/SWE observations. *Geophys. Res. Lett*. **33** (9).

HELLINGER, P., TRÁVNÍČEK, P.M., ŠTVERÁK, Š., MATTEINI, L. & VELLI, M. 2013 Proton thermal energetics in the solar wind: helios reloaded. *J. Geophys. Res*. **118** (4), 1351–1365.

HNAT, B., CHAPMAN, S.C., KIYANI, K., ROWLANDS, G. & WATKINS, N.W. 2007 On the fractal nature of the magnetic field energy density in the solar wind. *Geophys. Res. Lett*. **34** (15).

HORBURY, T.S., O'BRIEN, H., CARRASCO BLAZQUEZ, I., BENDYK, M., BROWN, P., HUDSON, R., EVANS, V., ODDY, T.M., CARR, C.M., BEEK, T.J., *et al.* 2020 The solar orbiter magnetometer. *Astron. Astrophys*. **642**, A9.

HORBURY, T.S., WICKS, R.T. & CHEN, C.H.K. 2012 Anisotropy in space plasma turbulence: solar wind observations. *Space Sci. Rev*. **172** (1–4), 325–342.

HOWES, G.G. 2015 A dynamical model of plasma turbulence in the solar wind. *Phil. Trans. R. Soc.* A **373** (2041), 20140145.

ISENBERG, P.A., MARUCA, B.A. & KASPER, J.C. 2013 Self-consistent ion cyclotron anisotropy-beta relation for solar wind protons. *Astrophys. J*. **773** (2), 164.

KASPER, J.C., LAZARUS, A.J. & GARY, S.P. 2002 Wind/SWE observations of firehose constraint on solar wind proton temperature anisotropy. *Geophys. Res. Lett*. **29** (17), 20-1–20-4.

KIYANI, K., CHAPMAN, S.C. & HNAT, B. 2006 Extracting the scaling exponents of a self-affine, non-Gaussian process from a finite-length time series. *Phys. Rev.* E **74** (5), 051122.

KIYANI, K.H., OSMAN, K.T. & CHAPMAN, S.C. 2015 Dissipation and heating in solar wind turbulence: from the macro to the micro and back again. *Phil. Trans. R. Soc.* A **373** (2041), 20140155.

KLEIN, K.G., SPENCE, H., ALEXANDROVA, O., ARGALL, M., ARZAMASSKIY, L., BOOKBINDER, J., BROEREN, T., CAPRIOLI, D., CASE, A., CHANDRAN, B., *et al.* 2023 HelioSwarm: a multipoint, multiscale mission to characterize turbulence. *Space Sci. Rev*. **219** (8), 74.

KOLMOGOROV, A.N. 1941 Dissipation of energy in locally isotropic turbulence. *Dokl. Akad. Nauk SSSR* **32**, 16.

KULSRUD, R.M. 1984 MHD description of plasma. In *Basic Plasma Physics: Selected Chapters, Handbook of Plasma Physics*, vol. 1, p. 115. North-Holland Publishing Company. ADS Bibcode: 1984bpp..conf..115K.

KUNZ, M.W., SCHEKOCHIHIN, A.A. & STONE, J.M. 2014 Firehose and mirror instabilities in a collisionless shearing plasma. *Phys. Rev. Lett*. **112** (20), 205003.

LOUARN, P., FEDOROV, A., PRECH, L., OWEN, C.J., BRUNO, R., LIVI, S., LAVRAUD, B., ROUILLARD, A.P., GENOT, V., ANDRE, N., *et al.* 2021 Multiscale views of an Alfvénic slow solar wind: 3D velocity distribution functions observed by the Proton-Alpha Sensor of Solar Orbiter. *Astron. Astrophys*. **656**, A36.

MARINO, R. & SORRISO-VALVO, L. 2023 Scaling laws for the energy transfer in space plasma turbulence. *Phys. Rep*. **1006**, 1–144.

MARKOVSKII, S.A. & VASQUEZ, B.J. 2022 The effect of solar wind turbulence on parallel and oblique firehose instabilities. *Astrophys. J*. **924** (2), 111.

MARSCH, E., MÜHLHÄUSER, K.-H., SCHWENN, R., ROSENBAUER, H., PILIPP, W. & NEUBAUER, F.M. 1982 Solar wind protons: three-dimensional velocity distributions and derived plasma parameters measured between 0.3 and 1 AU. *J. Geophys. Res*. **87** (A1), 52–72.

MARSCH, E. & TU, C.-Y. 1997 Intermittency, non-Gaussian statistics and fractal scaling of MHD fluctuations in the solar wind. *Nonlinear Process. Geophys*. **4** (2), 101–124.

MARUCA, B.A., KASPER, J.C. & BALE, S.D. 2011 What are the relative roles of heating and cooling in generating solar wind temperature anisotropies? *Phys. Rev. Lett*. **107** (20), 201101.

MATTEINI, L., HELLINGER, P., LANDI, S., TRÁVNÍČEK, P.M. & VELLI, M. 2012 Ion kinetics in the solar wind: coupling global expansion to local microphysics. *Space Sci. Rev*. **172** (1–4), 373–396.

MATTEINI, L., LANDI, S., HELLINGER, P., PANTELLINI, F., MAKSIMOVIC, M., VELLI, M., GOLDSTEIN, B.E. & MARSCH, E. 2007 Evolution of the solar wind proton temperature anisotropy from 0.3 to 2.5 AU. *Geophys. Res. Lett*. **34** (20), L20105.

MATTHAEUS, W.H., WAN, M., SERVIDIO, S., GRECO, A., OSMAN, K.T., OUGHTON, S. & DMITRUK, P. 2015 Intermittency, nonlinear dynamics and dissipation in the solar wind and astrophysical plasmas. *Phil. R. Soc.* A **373** (2041), 20140154.

MÖSTL, C., ISAVNIN, A., BOAKES, P.D., KILPUA, E.K.J., DAVIES, J.A., HARRISON, R.A., BARNES, D., KRUPAR, V., EASTWOOD, J.P., GOOD, S.W., *et al.* 2017 Modeling observations

https://doi.org/10.1017/S0022377824001375 Published online by Cambridge University Press

of solar coronal mass ejections with heliospheric imagers verified with the Heliophysics System Observatory. *Space Weath*. **15** (7), 955–970.

Möstl, C., Weiss, A.J., Bailey, R.L., Reiss, M.A., Amerstorfer, T., Hinterreiter, J., Bauer, M., McIntosh, S.W., Lugaz, N. & Stansby, D. 2020 Prediction of the In Situ Coronal Mass Ejection Rate for Solar Cycle 25: Implications for Parker Solar Probe In Situ Observations. *Astrophys. J*. **903** (2), 92.

Opie, S., Verscharen, D., Chen, C.H.K., Owen, C.J. & Isenberg, P.A. 2022 Conditions for proton temperature anisotropy to drive instabilities in the solar wind. *Astrophys. J*. **941** (2), 176.

Opie, S., Verscharen, D., Chen, C.H.K., Owen, C.J. & Isenberg, P.A. 2023 The effect of variations in the magnetic field direction from turbulence on kinetic-scale instabilities. *Astron. Astrophys*. **672**, L4.

Osman, K.T., Matthaeus, W.H., Hnat, B. & Chapman, S.C. 2012 Kinetic signatures and intermittent turbulence in the solar wind plasma. *Phys. Rev. Lett*. **108** (26), 261103.

Osman, K.T., Matthaeus, W.H., Kiyani, K.H., Hnat, B. & Chapman, S.C. 2013 Proton kinetic effects and turbulent energy cascade rate in the solar wind. *Phys. Rev. Lett*. **111** (20), 201101.

Oughton, S., Matthaeus, W.H., Wan, M. & Osman, K.T. 2015 Anisotropy in solar wind plasma turbulence. *Phil. Trans. R. Soc.* A **373** (2041), 20140152.

Owen, C.J., Bruno, R., Livi, S., Louarn, P., Al Janabi, K., Allegrini, F., Amoros, C., Baruah, R., Barthe, A., Berthomier, M., *et al.* 2020 The solar orbiter solar wind analyser (SWA) suite. *Astron. Astrophys*. **642**, A16.

Paladin, G. & Vulpiani, A. 1987 Anomalous scaling laws in multifractal objects. *Phys. Rep*. **156** (4), 147–225.

Parashar, T.N., Shay, M.A., Cassak, P.A. & Matthaeus, W.H. 2009 Kinetic dissipation and anisotropic heating in a turbulent collisionless plasma. *Phys. Plasmas* **16** (3), 032310.

Politano, H. & Pouquet, A. 1998 von Kármán–Howarth equation for magnetohydrodynamics and its consequences on third-order longitudinal structure and correlation functions. *Phys. Rev.* E **57** (1), R21–R24.

Qudsi, R.A., Maruca, B.A., Matthaeus, W.H., Parashar, T.N., Bandyopadhyay, R., Chhiber, R., Chasapis, A., Goldstein, M.L., Bale, S.D., Bonnell, J.W., *et al.* 2020 Observations of heating along intermittent structures in the inner heliosphere from *PSP* data. *Astrophys. J. Suppl. Ser*. **246** (2), 46.

Retinò, A., Khotyaintsev, Y., Le Contel, O., Marcucci, M.F., Plaschke, F., Vaivads, A., Angelopoulos, V., Blasi, P., Burch, J., De Keyser, J., *et al.* 2022 Particle energization in space plasmas: towards a multi-point, multi-scale plasma observatory. *Expl Astron*. **54** (2), 427–471.

Rouillard, A.P., Pinto, R.F., Vourlidas, A., De Groof, A., Thompson, W.T., Bemporad, A., Dolei, S., Indurain, M., Buchlin, E., Sasso, C., *et al.* 2020 Models and data analysis tools for the solar orbiter mission. *Astron. Astrophys*. **642**, A2.

Schekochihin, A.A. 2022 MHD turbulence: a biased review. *J. Plasma Phys*. **88** (5), 155880501.

Schekochihin, A.A., Cowley, S.C., Dorland, W., Hammett, G.W., Howes, G.G., Quataert, E. & Tatsuno, T. 2009 Astrophysical gyrokinetics: kinetic and fluid turbulent cascades in magnetized weakly collisional plasmas. *Astrophys. J. Suppl. Ser*. **182** (1), 310–377.

Servidio, S., Osman, K.T., Valentini, F., Perrone, D., Califano, F., Chapman, S., Matthaeus, W.H. & Veltri, P. 2014 Proton kinetic effects in vlasov and solar wind turbulence. *Astrophys. J*. **781** (2), L27.

Simon, P. & Sahraoui, F. 2022 Exact law for compressible pressure-anisotropic magnetohydrodynamic turbulence: toward linking energy cascade and instabilities. *Phys. Rev.* E **105** (5), 055111.

Sorriso-Valvo, L., Carbone, F., Leonardis, E., Chen, C.H.K., Šafránková, J. & Němeček, Z. 2017 Multifractal analysis of high resolution solar wind proton density measurements. *Adv. Space Res*. **59** (6), 1642–1651.

Sorriso-Valvo, L., Carbone, F., Perri, S., Greco, A., Marino, R. & Bruno, R. 2018*a* On the statistical properties of turbulent energy transfer rate in the inner heliosphere. *Sol. Phys*. **293** (1), 10.

Sorriso-Valvo, L., Carbone, V., Veltri, P., Consolini, G. & Bruno, R. 1999 Intermittency in the solar wind turbulence through probability distribution functions of fluctuations. *Geophys. Res. Lett*. **26** (13), 1801–1804.

SORRISO-VALVO, L., CATAPANO, F., RETINO, A., LE CONTEL, O., PERRONE, D., ROBERTS, O.W., COBURN, J.T., PANEBIANCO, V., VALENTINI, F., PERRI, S., *et al.* 2019 Turbulence-driven ion beams in the magnetospheric Kelvin–Helmholtz instability. *Phys. Rev. Lett*. **122** (3), 035102.

SORRISO-VALVO, L., PERRONE, D., PEZZI, O., VALENTINI, F., SERVIDIO, S., ZOUGANELIS, I. & VELTRI, P. 2018*b* Local energy transfer rate and kinetic processes: the fate of turbulent energy in two-dimensional hybrid Vlasov–Maxwell numerical simulations. *J. Plasma Phys*. **84** (2), 725840201.

SQUIRE, J., KUNZ, M.W., ARZAMASSKIY, L., JOHNSTON, Z., QUATAERT, E. & SCHEKOCHIHIN, A.A. 2023 Pressure anisotropy and viscous heating in weakly collisional plasma turbulence. *J. Plasma Phys*. **89** (4), 905890417.

SQUIRE, J., QUATAERT, E. & SCHEKOCHIHIN, A.A. 2016 A stringent limit on the amplitude of Alfvénic perturbations in high-beta low-collisionality plasmas. *Astrophys. J. Lett*. **830** (2), L25.

SQUIRE, J., SCHEKOCHIHIN, A.A. & QUATAERT, E. 2017 Amplitude limits and nonlinear damping of shear-Alfvén waves in high-beta low-collisionality plasmas. *New J. Phys*. **19** (5), 055005.

TAYLOR, G.I. 1938 The spectrum of turbulence. *Proc. R. Soc.* A **164** (919), 476–490.

TU, C.-Y. & MARSCH, E. 1995 MHD structures, waves and turbulence in the solar wind: observations and theories. *Space Sci. Rev*. **73** (1–2), 1–210.

VERSCHAREN, D., CHANDRAN, B.D.G., KLEIN, K.G. & QUATAERT, E. 2016 Collisionless isotropization of the solar-wind protons by compressive fluctuations and plasma instabilities. *Astrophys. J*. **831** (2), 128.

VERSCHAREN, D., KLEIN, K.G. & MARUCA, B.A. 2019 The multi-scale nature of the solar wind. *Liv. Rev. Sol. Phys*. **16** (1).

WICKS, R.T., HORBURY, T.S., CHEN, C.H.K. & SCHEKOCHIHIN, A.A. 2011 Anisotropy of imbalanced Alfvénic turbulence in fast solar wind. *Phys. Rev. Lett*. **106** (4), 045001.

YANG, Y., MATTHAEUS, W.H., PARASHAR, T.N., HAGGERTY, C.C., ROYTERSHTEYN, V., DAUGHTON, W., WAN, M., SHI, Y. & CHEN, S. 2017 Energy transfer, pressure tensor, and heating of kinetic plasma. *Phys. Plasmas* **24** (7), 072306.

YANG, Y., PECORA, F., MATTHAEUS, W.H., ROY, S., CUESTA, M.E., CHASAPIS, A., PARASHAR, T., BANDYOPADHYAY, R., GERSHMAN, D.J., GILES, B.L., *et al.* 2023 Quantifying the agyrotropy of proton and electron heating in turbulent plasmas. *Astrophys. J*. **944** (2), 148.